ACS APPLIED ENERGY MATERIALS

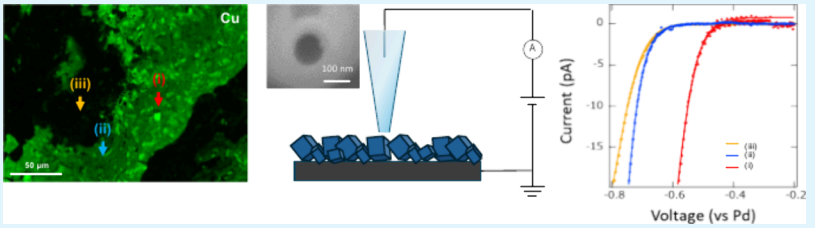
www.acsaem.org Article

# Crystalline Formation Enhances Hydrogen Evolution Reaction Property of Copper Azaphthalocyanine on Carbon Electrodes

Kosuke Ishibashi, Tengyi Liu, Yuya Ishizaki, Shusaku Nagano, Junya Yoshida, Shimpei Ono, Yasufumi Takahashi, Akichika Kumatani,* and Hiroshi Yabu*

Cite This: *ACS Appl. Energy Mater.* 2024, 7, 10466−10473 Read Online

ACCESS | Metrics & More | Article Recommendations | Supporting Information




**ABSTRACT:** Alkaline water electrolysis and alkaline exchange membrane (AEM) water electrolysis are expected to be next-generation hydrogen generation devices due to their low corrosion, high efficiency, and low maintenance costs. The performance of the electrode catalyst is especially important as it directly affects the overvoltage of water electrolysis, and platinum (Pt), a rare metal, has traditionally been used as a catalyst for the hydrogen evolution reaction (HER) due to its direct impact on the overvoltage of hydrogen generation. However, due to resource constraints and rising costs, the development of alternative catalysts is underway. In this study, the formation of copper azaphthalocyanine (CuAzPc-4N) was directly coated on a carbon electrode as a HER catalyst. X-ray analysis and microscopic measurements revealed crystalline formation at high loading conditions. Scanning electrochemical cell microscopy showed that morphological differences were found in the samples with alternating coating times, and the crystal of CuAzPc-4N exhibits higher HER activity than its molecular state.

**KEYWORDS:** *hydrogen evolution reaction, metal azaphthalocyanine, crystalline, carbon, scanning electrochemical cell microscopy*

## 1. INTRODUCTION

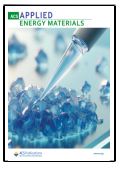
To achieve a hydrogen society, water electrolysis systems using renewable energy are gaining attention.[1,2] Alkaline water electrolysis and AEM water electrolysis are expected to be next-generation hydrogen generation devices due to their low corrosion, high efficiency, and low maintenance costs.[3] Various factors influence the performance of water electrolysis, but the performance of the electrode catalyst is especially important as it directly affects the overvoltage of water electrolysis.[4] Platinum (Pt), a rare metal, has traditionally been used as a catalyst for the hydrogen evolution reaction (HER) due to its direct impact on the overvoltage of hydrogen generation. However, due to resource constraints and rising costs, the development of alternative catalysts is underway.

Many HER catalysts have been proposed so far. In alkaline water electrolysis, metals with low resistance, such as nickel (Ni) and their alloys,[5] have mainly been used to carry high currents through the electrodes. On the other hand, in the case of AEM type, the formation of a three-layer interface is important, so electrodes with catalysts supported on a hydrophobic carbon paper are used. Similar to fuel cells, Pt/C,[6] $MoS_2$,[7] and carbon alloy catalysts[8−13] have been proposed as HER catalysts.

Metal phthalocyanines, which are chemically, thermally, and electrically robust among organic materials, are used as organic semiconductors in energy conversion materials.[14,15] In recent years, metal phthalocyanines have also attracted attention as various electrochemical catalysts. The advantage of metal phthalocyanines is the designability of molecular structures to control adsorption potentials of reactive substrates to the active site metals. This designability allows them to apply wide variety of various electrochemical processes, and several metal phthalocyanines have been proposed as HER catalysts with changing centric metals such as iron,[16] cobalt,[17] and copper.[18]

We have been developing electrocatalysts using metal azaphthalocyanines, a type of metal phthalocyanine, due to their high activity as oxygen reduction reaction (ORR) catalysts and their solubility to organic solvents. We have found that catalysts containing iron azaphthalocyanine (FeAzPc-4N) molecularly attached onto porous carbons are

**Received:** August 15, 2024
**Revised:** October 17, 2024
**Accepted:** October 29, 2024
**Published:** November 8, 2024



Downloaded from pubs.acs.org/aaemcq/article-pdf/7/22/10466/18573985/ae4c02102.pdf by DOKUZ EYLUL UNIV user on 01 September 2026


© 2024 American Chemical Society

https://doi.org/10.1021/acsaem.4c02102
*ACS Appl. Energy Mater.* 2024, 7, 10466−10473

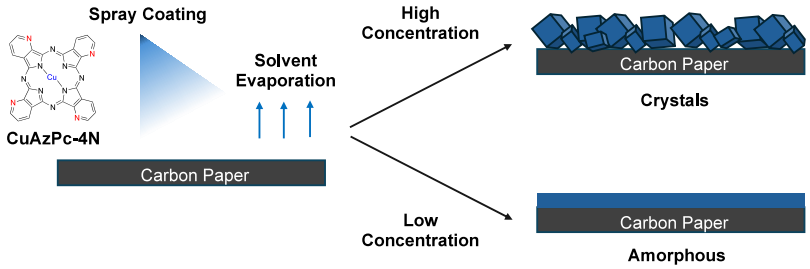



**Figure 1.** Schematic illustration of the sample electrode preparation.

useful for ORR,[19−23] HER electrocatalysts,[24] and pseudocapacitance in capacitors.[25]

In these existing studies, various states of catalyst loading on the electrodes have been investigated. Some reports simply mix catalyst powders[26] with carbon, while others immobilized molecules on porous carbon through molecular adsorption.[27−29] In addition, covalent organic frameworks (COFs) of metal phthalocyanines also employed to immobilize catalytic sites on the surface.[30,31] However, there are few papers that discuss the impact of the immobilized state of single metal phthalocyanine molecules on the HER activity.

Copper azaphthalocyanine (CuAzPc-4N) showed lower ORR and HER activity compared to iron;[24] however, when it was directly coated CuAzPc-4N on a carbon electrode at different concentrations and the HER activity was measured, it was observed that the HER activity increased with increasing coating concentrations. Compared to Pt/C and $MoS_2$, metal complex molecular catalysts such as CuAzPc-4N have the following advantages:

1. They are not affected by resource constraints. Both Pt and Mo have low crystal abundances and require significant energy for extraction. In contrast, metal complex molecular catalysts are composed of transition metals and organic materials, making them less susceptible to resource limitations.
2. They are cost-effective. CuAzPc-4N is commonly available as a blue pigment and can be synthesized at a much lower cost compared to catalysts that use elements like Pt or Mo.
3. They reduce the amount of metals required. Conventional catalysts often consist of nanoparticles of metals or metal compounds, where only the surface metal is active and the metal inside the nanoparticles does not contribute to catalytic activity. By utilizing metal complexation, it is possible to increase the efficiency of metal usage and improve elemental efficiency.

In this paper, we report the formation of CuAzPc-4N crystals at high concentration regions determined by X-ray diffraction (XRD), glazing angle small-angle X-ray scattering (GISAXS), and electron probe micro analyzer (EPMA) measurements, and scanning electrochemical cell microscopy (SECCM) showed that the crystal of CuAzPc-4N exhibits higher HER activity than its molecular state.

## 2. MATERIALS AND METHODS

**2.1. Materials.** CuAzPc-4N was synthesized according to the literature[24] (see Supporting Information, S1) and kindly provided by AZUL Energy, Inc. Dimethyl sulfoxide (DMSO), isopropanol (IPA), and $H_2SO_4$ were purchased from Fujifilm Wako Pure Chemical Corporation, Osaka, Japan.

**2.2. Electrochemical Measurements.** CuAzPc-4N-coated carbon papers were prepared by spray coating of a DMSO/IPA solution of CuAzPc-4N. 1.1 mg/mL DMSO/IPA solution of CuAzPc-4N spray-coated (SimCoat, Sono-Tek Corporation, Milton, NY, USA) onto a carbon paper (MFK-A,Mitsubishi Chemical Corp.) substrate to fabricate a catalyst-coated sheet to prepare 1 time to 20 times coated carbon papers (Figure 1). The catalyst loading was measured by measuring before/after the weight of the sample electrode (Table 1).

**Table 1. Coating Times, Catalyst Loadings, and Overpotential Values ($\eta$) of the Prepared Samples**

| coating times | loading ($\mu$g/cm$^2$) | $\eta_{@j=10\ mA/cm2}$ [$V$ vs RHE] | $\eta_{@j=800\ mA/cm2}$ [$V$ vs RHE] |
|---|---|---|---|
| 1 | 21.4 | 0.578 | 3.31 |
| 2 | 42.8 | 0.637 | 3.50 |
| 4 | 85.6 | 0.549 | 2.97 |
| 8 | 171 | 0.518 | 2.62 |
| 12 | 257 | 0.521 | 2.63 |
| 14 | 297 | 0.570 | 2.82 |
| 16 | 342 | 0.583 | 2.74 |
| 18 | 385 | 0.611 | 2.82 |
| 20 | 428 | 0.594 | 2.99 |

The electrochemical experiments were conducted using a three-electrode cell setup, utilizing a VersaSTAT 4 instrument (Ametek, Berwyn, PA, USA). Linear sweep voltammetry (LSV) curves of HER in 0.5 M $H_2SO_4$aq. were measured by a three-electrode type beaker cell using Pt wire as a counter electrode (CE), Ag/AgCl as a reference electrode (RE), and samples fixed in an electrode holder (AE-9, EC frontier, Japan) as a working electrode (WE), respectively. The potential versus Ag/AgCl was converted to the reversible hydrogen electrode (RHE) scale using the following equation:

$$E\ (\text{vs RHE}) = E\ (\text{vs Ag/AgCl}) + 0.197 + 0.059\ \text{V·pH}$$

**2.3. EPMA Measurements.** The surface morphologies and elemental mapping of the sample electrodes were observed by using an electron probe micro analyzer (EPMA, JXA-8530F, JEOL, Tokyo, Japan).

**2.4. X-ray Analysis.** XRD of blank (Si(100)), 1 time, and 20 times CuAzPc-4N-coated carbon papers was measured by SmartLab 9MTP, RIGAKU, Japan. GISAXS measurements were carried out with an X-ray diffractometer (NANOPIX, Rigaku, Tokyo, Japan) using Cu K$\alpha$ radiation ($\lambda$ = 0.154 nm) with a camera length of 360 mm for 15 min of irradiation time.

X-ray absorption near edge structure (XANES) in XAFS spectra of CuAzPc-4N coated on carbon papers with different coating times was measured by utilizing the BL08W beamline for hard X-ray absorption in NanoTerasu Synchrotron Light Source, Sendai, Japan. The spectra were analyzed using the "Athena" software package.

**2.5. SECCM Measurements.** Based upon the preceding bulk measurement data, it can be inferred that the significant electrochemical catalytic activity of the CuAzPc-4N is attributable to the microscale crystallization of CuAzPc-4N. Consequently, a detailed

Downloaded from pubs.acs.org/aaemcq/article-pdf/7/22/10466/18573985/ae4c02102.pdf by DOKUZ EYLUL UNIV user on 01 September 2026



https://doi.org/10.1021/acsaem.4c02102
ACS Appl. Energy Mater. 2024, 7, 10466−10473

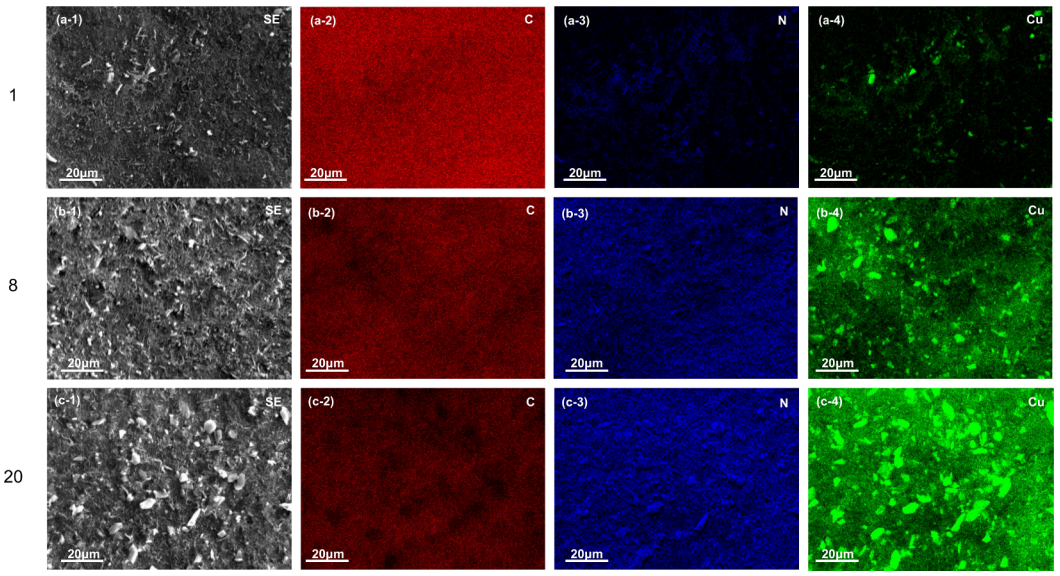



**Figure 2.** SE (a-1−c-1); elemental mapping images of C (a-2−c-2), N (a-3−c-3), and Cu (a-4−c-4) of 1 time coating (a-1−a-4); 8 times coating (b-1−b-4); and 20 times coating (c-1−c-4) measured by EPMA, respectively.

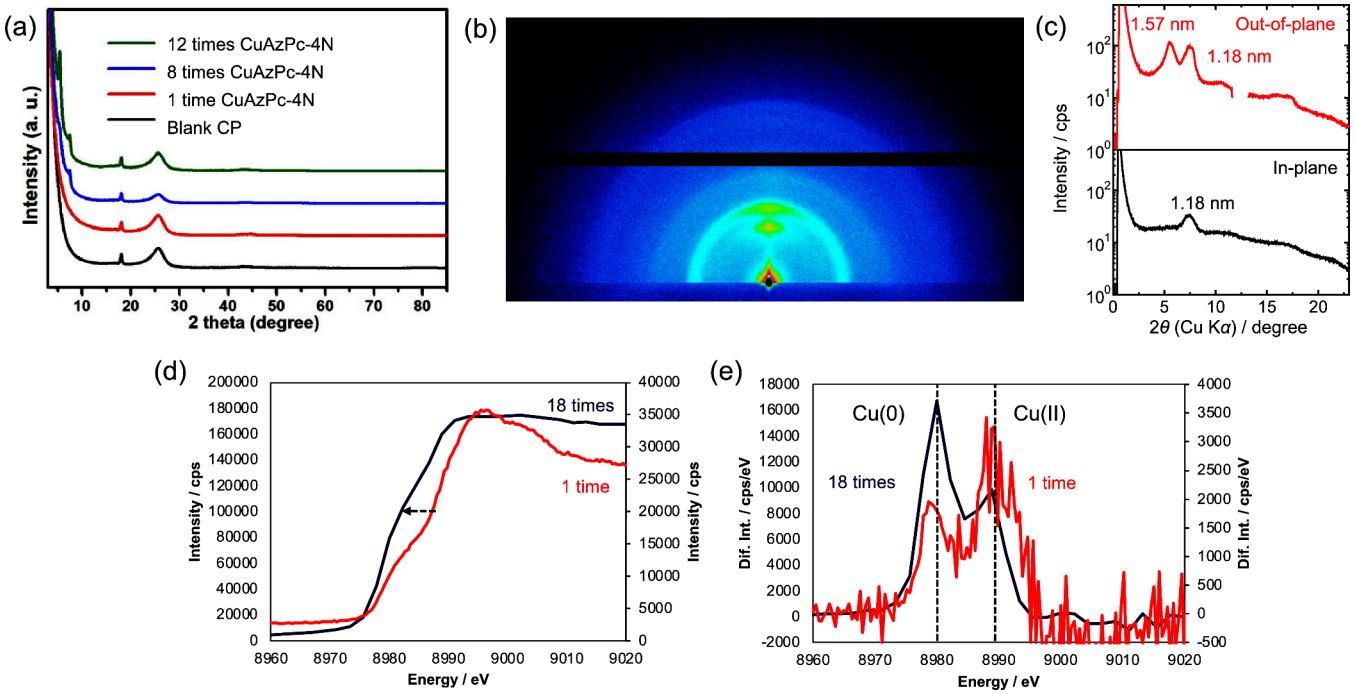



**Figure 3.** XRD results of blank CP, 1, 8, and 12 times CuAzPc-4N coated on CP (a) and GISAXS result of 12 times CuAzPc-4N coated on CP (b), respectively. (c) In-plane and out-of-plane intensities of (b). XANES (d) and differential of XANES intensity (e) of sample electrodes 1 time (red) and 18 times (black) coating, respectively.

examination was conducted using scanning electrochemical cell microscopy (SECCM) (see Supporting Information, S2), a scanning probe microscopic technique capable of measuring localized electrochemical reactions.[32] The SECCM utilizes a nanopipet filled with an electrolyte and a quasi-reference/counter electrode as a probe to create a droplet on the sample surface, enabling electrochemical cell measurements contingent on the aperture size of the pipet. Until date, the SECCM analysis has been employed to regulate edge effect in two-dimensional materials,[33] local chemical dopant effect,[9] and material functionalization.[34] In this work, the electrochemical catalytic activity was assessed by filling a nanopipet with 0.5 M $H_2SO_4$ and a palladium (Pd) wire, featuring an aperture diameter of approximately 100 nm, as shown in Supporting Information 1, to form droplets in both the amorphous and crystalline phases, respectively. The LSV measurements via those droplets on those phases were carried out at the scan speed of 100 mV/s under the same pipet.

## 3. RESULTS AND DISCUSSION

**3.1. Characterization of CuAzPc-4N-Coated Carbon Papers.** To clarify the state of the catalyst immobilized on the electrode, we performed structural and elemental mapping of the electrode surface using EPMA. Figure 2 shows the SE images (Figure 2a-1,b-1,c-1) and elemental mapping images of C (Figure 2a-2,b-2,c-2), N (Figure 2a-3,b-3,c-3), and Cu (Figure 2a-4,b-4,c-4) for electrodes with 1, 8, and 20 coating


https://doi.org/10.1021/acsaem.4c02102
ACS Appl. Energy Mater. 2024, 7, 10466−10473

Downloaded from pubs.acs.org/aaemcq/article-pdf/7/22/10466/18573985/ae4c02102.pdf by DOKUZ EYLUL UNIV user on 01 September 2026

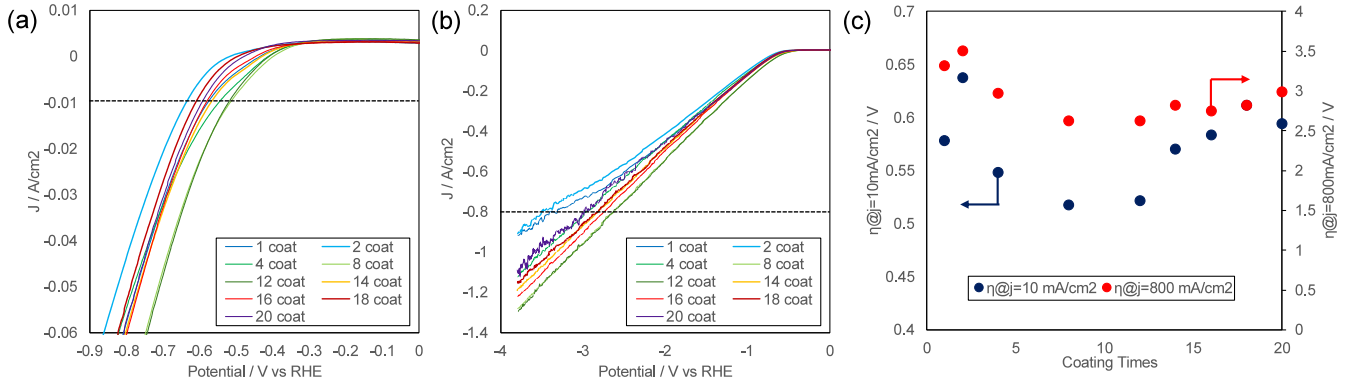



**Figure 4.** LSV curves of electrodes with different CuAzPc-4N coating times (a,b) and plot of overpotential values (c), respectively.

times. In the case of 1 time coating, there are small numbers of aggregates found in the SE image (Figure 2a-1) and signal from carbon was strongly imaged (Figure 2a-2). The weakly distributed signals of N and Cu (Figure 2a-3,a-4) were observed, and only small numbers of aggregates, which had high intensity of N and Cu signals, were found. On the other hand, as the coating time increases, signals from C decreased (Figure 2b-2,c-2), the number of aggregated structures in SE images increased (Figure 2b-1,c-1), and blight spots attributed to aggregates with high signal intensity of N and Cu were observed.

The coated catalyst is exposed to a large amount of solvent with each coating, and the repeated dissolution and precipitation process promotes crystallization of catalyst molecules. In the case of a single coating, the catalyst evaporates in a short amount of time, resulting in the precipitation of amorphous particles rather than crystallization. On the other hand, as the number of coatings increases, not only are additional catalyst molecules added but also the catalyst already deposited on the electrode also dissolves and reprecipitates, leading to high concentration of catalyst molecules locally that promotes crystallization. As a result, both the size and quantity of the crystals increase as the number of coatings rises.

From the image analysis of the EPMA measurement results, the size distribution of particles larger than 1 $\mu$m is presented in Supporting Information, S3. In the case of a single coating, most particles are fine particles smaller than 1 $\mu$m, and only a few micrometer-sized crystals were observed. In contrast, with 20 coatings, a lot of crystals with rectangular shapes were observed with the size exceeding 1 $\mu$m. This suggests that as the number of coatings increases, the crystallization process leads to higher number of formation and more mature crystalline particles.

Figure 3a shows the XRD data of carbon paper with varying coating times. In the blank and 1 time coating samples, only the diffraction peaks from the carbon paper are observed, while with increased coating times, diffraction peaks appear in the $2\theta < 10°$ region. To analyze these diffraction peaks in more detail, GISAXS analysis was performed on a 12 times spray-coated sample onto Si substrate (Figure 3b,c). As a result, diffraction peaks with $d$ = 1.18 nm in the in-plane direction and $d$ = 1.18, 1.57 nm, in the out-of-plane direction were observed. Referring to the crystal of CuPc,[35,36] this diffraction corresponds to the $\beta$-type crystal of CuAzPc-4N stacked in the out-of-plane direction. The $\beta$-type crystal structure was formed on the sample electrodes by spray coating.

Figure 3d shows the Cu−K edge XANES spectra of sample electrodes with 1 (red) and 18 (black) coatings, respectively. Interestingly, the shape of the XANES spectra significantly differs between 1 time and 18 times. At 1 time, an absorption band was observed with a peak around 8995 eV and a shoulder around 8980 eV, whereas at 18 times, the absorption edge shifted to the lower energy region. Figure 3e shows a plot of the derivative of the Figure 3d spectra. In the case of 1 time, there are peaks around 8980 and 8990 eV, corresponding to the absorption of Cu(0) and Cu(II), respectively, suggesting a higher proportion of Cu(II).[37] On the other hand, in the 18 times case, although the peak positions are similar, their ratios are reversed. This indicates that the electronic state of the catalytic center is affected by coating times. In order to elucidate the effect of coating times, we also analyzed EXAFS of samples with different coating times (see Supporting Information, S4). From the EXAFS results, Cu−N peaks are found in the range of 1.55−1.60 Å in both cases; however, the peak position was slightly moved to the larger atomic distance ($R$) position with increasing coating time. This implies that some portion of Cu in CuAzPc-4N changed from Cu(II) to Cu(I) or Cu(0), and this result supports the XANES data. In addition, the peak positions at the large R region over 2.0 Å, which reflected the local structures of peripheral groups of the azaphtalocyanine macrocycle, were much different when the coating times changed. The data imply that the catalytic center and peripheral structure changed, which induces the different electronic state with changing the coating times.

Results from EPMA, XRD, and GISAXS suggest that the difference in the number of coatings indicates a difference in the state of the catalytic molecules on the surface. When the number of coatings is low, the molecules are adsorbed on the surface directly onto the carbon, resulting in electrical interactions with the underlying carbon. Conversely, with a higher number of coatings, it became clear that the catalytic molecules crystallized. For the AZUL catalyst, which is a catalyst molecules adsorbed on carbon, UV photoelectron spectroscopy (UPS) measurements have revealed that the molecules adsorbed on carbon take on a different electronic state than in the crystal.[21] Therefore, the difference in the absorption edge observed in the XANES measurements with varying coating times suggests that the electronic state of the catalyst significantly changes due to interactions with the underlying carbon.

**3.2. LSV Curves of Electrodes with Different Coating Times.** The LSV curves of the HER in the low current region measured with electrodes spray-coated on a carbon paper as

Downloaded from pubs.acs.org/aaemcq/article-pdf/7/22/10466/1857398/ae4c02102.pdf by DOKUZ EYLUL UNIV user on 01 September 2026



https://doi.org/10.1021/acsaem.4c02102
ACS Appl. Energy Mater. 2024, 7, 10466−10473

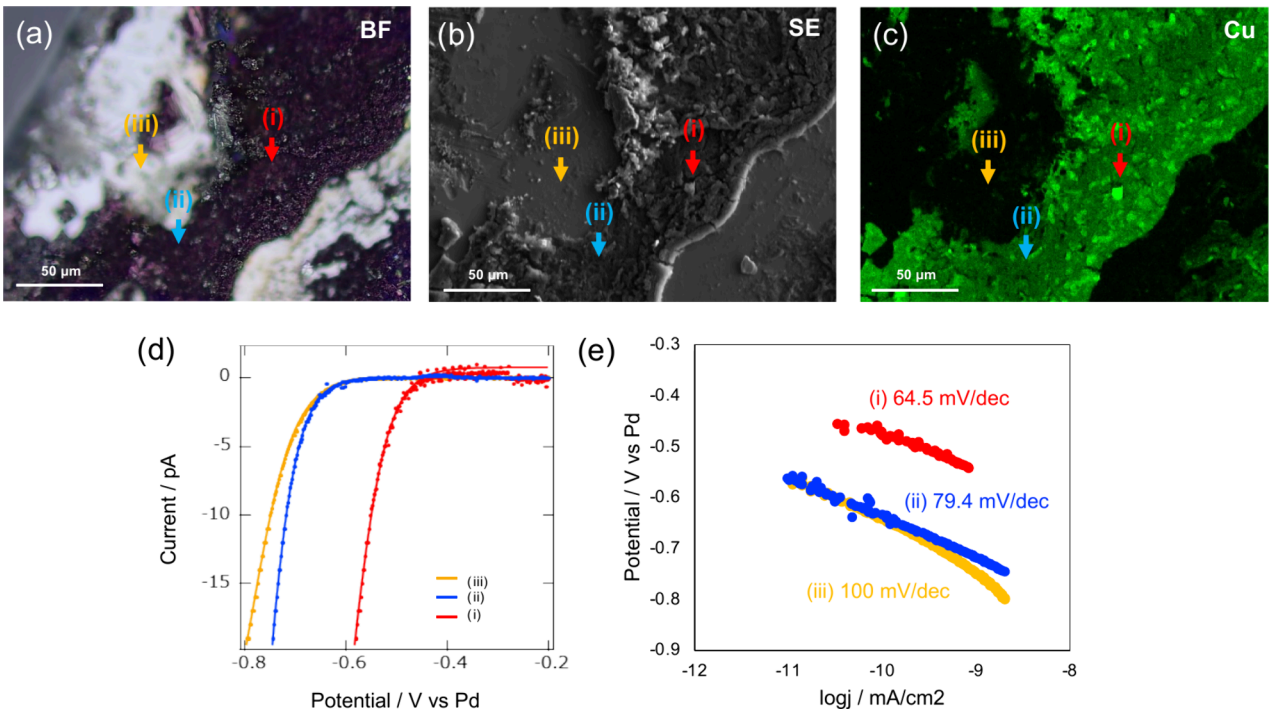



**Figure 5.** Optical micrograph (a), SE (b), and Cu mapping (c) images of a cast sample, LSV curves (d), and Tafel slope (e) obtained by SECCM measurements, respectively.

the WE are shown in Figure 4a. When the coating times was low, the potential at 10 mA/cm$^2$ ($E_{@j=10\ mA/cm2}$) was low, and it was around −0.6 V vs RHE. However, as the coating times increased, the potential rose, reaching up to −0.518 V vs RHE with eight times coating (Table 1). On the other hand, beyond 14 times, the potential decreased. It is well-known that Pt/C shows high HER performance and the onset potential of HER is normally 0 V vs RHE. From the previous work, we have reported $E_{@j=10\ mA/cm2}$ (Pt/C) was −0.035 V vs RHE.[24] On the other hand, the minimum $E_{@j=10\ mA/cm2}$ (CuAzPc-4N) was −0.518 V vs RHE, which was much higher overpotential than that of Pt/C. It is still challenging that such single atom molecular catalyst to improve the performance, however, the finding reported in this manuscript, the crystal structure enhances the performance of HER, gives important insight to improve the performance of molecular catalyst for HER.

Figure 4b shows the LSV curves of HER measured up to the high current region. Comparing the potentials at 800 mA/cm$^2$ ($E_{@j=800\ mA/cm2}$), the activity in the high current region was particularly low when the amount of catalyst was small. The activity increased with 8−12 coats but decreased again beyond that, correlating with the activity in the low current region.

Figure 4c plots the reaction overpotentials at $j$ = 10 mA/cm$^2$ ($\eta_{@j=10\ mA/cm2}$) and at $j$ = 800 mA/cm$^2$ ($\eta_{@j=800\ mA/cm2}$) based on these results. It was evident that the reaction overpotential significantly decreased with 8−12 coats. This result indicates that even though the catalyst molecules are the same as CuAzPc-4N, the state of the coated catalyst affects the HER activity.

From the previous work,[24] we found that the performance of CuAzPc-4N was not enough as a HER catalyst in the full cell evaluation; therefore, the new way for improving the HER performance of molecular electrocatalyst was demanded. This work shows that the crystalline structure of the molecular catalyst has a potential for improving the HER performance, and this is one of the key findings in this paper.

**3.3. SECCM Analysis.** To microscopically clarify the difference in HER activity between the crystalline and other regions, SECCM measurements were performed. When CuAzPc-4N was cast on the substrate, a sample with mixed crystalline and amorphous regions was formed. As observed by optical microscopy (Figure 5a) and EPMA (Figure 5b,c), the sample surface was classified into high reflection intensity crystalline regions (i) with strong Cu signals in the elemental mapping image, low reflection intensity amorphous regions (ii) with weak Cu signals, and the substrate (iii).

The LSV measurements at each location are shown in Figure 5d. Compared to the substrate region (iii), the amorphous region (ii) showed almost no change in the onset potential, but the current value slightly increased. On the other hand, the crystalline region (i) showed a clear improvement in the onset potential. This indicates that even with the same CuAzPc-4N molecules, the HER catalytic activity varies depending on the aggregation state. From this result, it can be considered that the qualitative improvement of the HER activity on the electrode was brought about by the formation of crystalline states of CuAzPc-4N molecules.

Figure 5e shows the Tafel slope estimated from the LSV curves shown in Figure 5d. The reaction steps of HER are divided into the following three steps:

$$H_3O^+ + e^- \rightarrow H_{ads} + H_2O \text{ (Volmer step)}$$

$$H_{ads} + H_3O^+ + e^- \rightarrow H_2 + H_2O \text{ (Heyrovskystep)}$$

$$H_{ads} + H_{ads} \rightarrow H_2 \text{ (Tafelstep)}$$

The Tafel slope of substrate was 100 mV/dec, which indicates that the Volmer step is the rate limiting step and this is the first step of the HER, and therefore, the HER

Downloaded from pubs.acs.org/aaemcq/article-pdf/7/22/10466/1857398/ae4c02102.pdf by DOKUZ EYLUL UNIV user on 01 September 2026



https://doi.org/10.1021/acsaem.4c02102
ACS Appl. Energy Mater. 2024, 7, 10466−10473

performance of the substrate was quite low. On the other hand, Tafel slopes of amorphous and crystal regions were 79.4 and 64.5 mV/dec, respectively. Those values are attributed to Heyrovsky or Tafel steps. These results indicate that the reaction was smoothly conducted at the surface of CuAzPc-4N crystals.

**3.4. HER Enhancement Mechanisms.** From the above results, it was revealed that the crystals of CuAzPc-4N have higher HER activity compared to that of its amorphous molecular state. Based on the EPMA and XRD results, the number of crystals increases with the number of coatings, which explains the trend in overpotential observed in Figure 2c as follows: With fewer coating times, CuAzPc-4N is mainly coated on the carbon paper in a molecular or amorphous state, with very few crystals existence. Since the SECCM analysis shows that the amorphous structure has HER activity lower than that of crystals, the HER activity is low when this structure is predominant. It is well-known that the valence of catalytic center Cu dominates the electrocatalytic process of HER[38] because the HER process is mainly catalyzed by Cu redox.[39] From the Tafel slope result, the reaction on the amorphous state was dominated by the reduction process of hydrogen ion on the catalyst center. XANES analysis of 1 time coating sample revealed that Cu(II) was the main component of the catalytic center; therefore, the catalyst was difficult to donate electron to hydrogen ion. On the other hand, as the number of coating times increases, the number of crystalline grains with high HER activity also increases. From the XANES result of 18 times coating, Cu(0) was the main component of the catalytic center that easily gives electrons from electrode to adsorbed hydrogen ion compared with the Cu(II) at the amorphous state. In addition, the crystalline structure that makes the distance closer between catalytic centers, which results in the rate limiting process, was confirmed by the Tafel slope result. Therefore, the overpotential gradually decreases, achieving the highest HER activity with 8−12 coatings. Further increasing the number of coating times leads to a decrease in the carbon signal on the surface, as measured by EPMA, indicating a decrease of surface conductivity. As a result, it becomes more difficult for the current to flow to realize an efficient HER, and the activity decreases again.

From the results of the CV (see Supporting Information in S5), reduction peaks were observed around −0.3 V vs RHE in all cases. Compared to the 1 time coating, the reduction peak for the 12 times and 18 times coatings showed a greater drop, suggesting that the reaction occurs more efficiently. On the other hand, oxidation peaks were not observed in the 1 time coating, but they were detected in the 12 times and 18 times coatings. Furthermore, when the CV was repeated, the absolute value of the current gradually decreased in the 1 time coating, whereas no such decrease was observed in the 12 times and 18 times coatings. This suggests that in the case of the 1 time coating, the catalyst does not return to its original electronic state, while in the 12 times and 18 times coatings, repeated reactions are possible. Combined with the XANES and EXAFS data, in the 1 time coating, where the Cu(II) state is dominant, hydrogen evolution reaction (HER) is less likely to occur, and even when it occurs, the catalyst is oxidized and does not return to its original state, resulting in a decline in activity. In contrast, in the 12 times and 18 times coatings, repeated redox reactions occur, suggesting that HER activity is maintained without being lost, leading to stable catalytic performance.

In addition, it has been suggested that current measurements in SECCM are influenced by the density of electronic states (DOS) at different energy levels when the material is a semiconductor or conductor.[40] For example, even if the material is the same, local variations in DOS, such as in the structure of graphene[41,42] or structural defects in two-dimensional materials,[43] can affect electrochemical reactions. In the case of this study, as the material crystallizes, the DOS changes, and this change can be observed electrochemically by using SECCM. As a result, high catalytic activity was observed.

## 4. CONCLUSIONS

This study revealed several key findings from the SECCM and electrochemical analysis: the HER activity of CuAzPc-4N is higher in its crystalline form compared to its amorphous molecular state; it is possible to apply it in a crystalline form on a carbon paper through spray coating; and even in its crystalline form, excessive amounts lead to decrease in performance. The main finding of this paper is that the crystalline Cu-AzPc-4N exhibits higher HER activity as compared to its amorphous form.

There have been many attempts to increase the catalytic activity by increasing the number of active sites through the molecular adsorption of metal complex molecules on carbon. However, there are very few reported cases in which the catalytic activity of metal complex molecules increases by forming crystals. This study highlights the importance of crystal engineering, including crystallization, in the catalyst design of metal complex molecules. Future studies, combining both theoretical and experimental approaches, including DFT calculations, are expected to provide more detailed insights.

## ■ ASSOCIATED CONTENT

### Supporting Information

The Supporting Information is available free of charge at https://pubs.acs.org/doi/10.1021/acsaem.4c02102.

Synthetic route of CuAzPc-4N, schematic illustration of SECCM analysis, size distribution of CuAzPc-4N crystals, EXAFS data, and CV of CuAzPc-4N on carbon papers with different coating times (PDF)

## ■ AUTHOR INFORMATION


### Corresponding Authors

**Akichika Kumatani** − *Advanced Institute for Materials Research (WPI-AIMR), Tohoku University, Sendai 980-8577, Japan; Department of Electrical and Electronic Engineering, Chiba Institute of Technology, Chiba 275-0016, Japan; Graduate School of Engineering and Center for Science and Innovation in Spintronics, Tohoku University, Miyagi 980-8577, Japan; Precursory Research for Embryonic Science and Technology, Japan Science and Technology Agency (JST), Saitama 332-0012, Japan*;
Email: kumatani.akichika@p.chibakoudai.jp

**Hiroshi Yabu** − *Advanced Institute for Materials Research (WPI-AIMR), Tohoku University, Sendai 980-8577, Japan*;
orcid.org/0000-0002-1943-6790;
Email: hiroshi.yabu.d5@tohoku.ac.jp

### Authors

**Kosuke Ishibashi** − *Advanced Institute for Materials Research (WPI-AIMR), Tohoku University, Sendai 980-8577, Japan*


Downloaded from pubs.acs.org/aaemcq/article-pdf/7/22/10466/18573985/ae4c02102.pdf by DOKUZ EYLUL UNIV user on 01 September 2026



https://doi.org/10.1021/acsaem.4c02102
ACS Appl. Energy Mater. 2024, 7, 10466−10473

**Tengyi Liu** − *Advanced Institute for Materials Research (WPI-AIMR), Tohoku University, Sendai 980-8577, Japan*
**Yuya Ishizaki** − *Department of Chemistry, College of Science, Rikkyo University, Tokyo 171-8501, Japan;* orcid.org/0000-0002-1243-0441
**Shusaku Nagano** − *Department of Chemistry, College of Science, Rikkyo University, Tokyo 171-8501, Japan;* orcid.org/0000-0002-3929-6377
**Junya Yoshida** − *International Center for Synchrotron Radiation Innovation Smart (SRIS), Tohoku University, Sendai 980-8572, Japan;* orcid.org/0000-0002-9398-746X
**Shimpei Ono** − *International Center for Synchrotron Radiation Innovation Smart (SRIS), Tohoku University, Sendai 980-8572, Japan*
**Yasufumi Takahashi** − *Department of Electronics, Graduate School of Engineering, Nagoya University, Aichi 464-8603, Japan; WPI-Nano Life Science Institute (NanoLSI), Kanazawa University, Kanazawa 920-1192, Japan;* orcid.org/0000-0003-2834-8300

Complete contact information is available at: https://pubs.acs.org/10.1021/acsaem.4c02102

### Author Contributions

K.I.: Validation, Investigation; T.L.: Validation, Investigation; Y.I.: Validation, Investigation; S.N.: Validation, Investigation; J.Y.: Investigation, Writing, Review and Editing; S.O.: Investigation, Writing, Review and Editing; Y.T.: Validation, Investigation; A.K.: Validation, Investigation, Conceptualization, Review and Editing; H.Y.: Conceptualization, Review and Editing, Writing, Supervision.

### Funding

This work has been partly supported by Advanced Target Project and Fusion research Grants, Tohoku University, Japan, KAKENHI, JSPS (Nos. JP23H00301, JP24H01189, JP24H00478, JP22K14731, 24K17741), JST-MIRAI Project (JPMJMI22I5), JST-FOREST (JPMJFR203 K), JST-PRESTO (JPMJPR2274), JST-CREST (JPMJCR21B5), JSPS Core-to-Core Program (JPJSCCA20220006), Hirose Foundation (The 10th Funding), The Asahi Glass Foundation, The Murata Science Foundation, and Toyota Mobility Foundation.

### Notes

The authors declare no competing financial interest.

## ■ ACKNOWLEDGMENTS

The authors would like to thank Dr. Yutaro Hirai, AZUL Energy, Inc. for synthesizing and providing CuAzPc-4N. The authors thank Dr. Kazutaka Kamitani, Photon Science Innovation Center, for helping XAFS analysis.

## ■ REFERENCES

(1) La Camera, F. *Making the Breakthrough: Green Hydrogen Policies and Technology Costs*; International Renewable Energy Agency, 2021.
(2) La Camera, F. *Green Hydrogen Cost Reduction: Scaling up Electrolysers to Meet the 1.50 C Climate Goal*; International Renewable Energy Agency, 2020.
(3) Du, N.; Roy, C.; Peach, R.; Turnbull, M.; Thiele, S.; Bock, C. Anion-Exchange Membrane Water Electrolyzers. *Chem. Rev.* **2022**, *122*, 11830−11895.
(4) Masel, R. I.; Liu, Z.; Sajjad, S. Anion Exchange Membrane Electrolyzers Showing 1 A/Cm 2 at Less Than 2 V. *ECS Trans* **2016**, *75* (14), 1143−1146.
(5) Jakšicjakšicá, J. M.; Vojnovićb, M. V.; Vojnovićb, V.; Krstajićb, N. V.; Krstajićb, K. Kinetic Analysis of Hydrogen Evolution at Ni-Mo Alloy Electrodes. *Electrochim. Acta* **2000**, *45*, 4151−4158.
(6) Guo, F.; Macdonald, T. J.; Sobrido, A. J.; Liu, L.; Feng, J.; He, G. Recent Advances in Ultralow-Pt-Loading Electrocatalysts for the Efficient Hydrogen Evolution. *Adv. Sci.* **2023**, *10*, No. 2301098.
(7) Qiao, S.; Zhao, J.; Zhang, B.; Liu, C.; Li, Z.; Hu, S.; Li, Q. Micrometer−Scale Biomass Carbon Tube Matrix Auxiliary MoS2 Heterojunction for Electrocatalytic Hydrogen Evolution. *Int. J. Hydrogen Energy* **2019**, *44* (60), 32019−32029.
(8) Zhang, X.; Yang, Z.; Yang, X.; Wang, Y.; Lu, Z. Engineering the Activity of CoNx-Graphene for Hydrogen Evolution. *Int. J. Hydrogen Energy* **2018**, *43* (45), 20573−20579.
(9) Kumatani, A.; Miura, C.; Kuramochi, H.; Ohto, T.; Wakisaka, M.; Nagata, Y.; Ida, H.; Takahashi, Y.; Hu, K.; Jeong, S.; Fujita, J.; Matsue, T.; Ito, Y. Chemical Dopants on Edge of Holey Graphene Accelerate Electrochemical Hydrogen Evolution Reaction. *Adv. Sci.* **2019**, *6* (10), No. 1900119.
(10) Pu, Z.; Amiinu, I. S.; Cheng, R.; Wang, P.; Zhang, C.; Mu, S.; Zhao, W.; Su, F.; Zhang, G.; Liao, S.; Sun, S. Single-Atom Catalysts for Electrochemical Hydrogen Evolution Reaction: Recent Advances and Future Perspectives. *Nanomicro Lett.* **2020**, *12* (1), 1−29.
(11) Wang, Q.; Guo, R.; Wang, Z.; Shen, D.; Yu, R.; Luo, K. H.; Wu, C.; Gu, S. Progress in Carbon-Based Electrocatalyst Derived from Biomass for the Hydrogen Evolution Reaction. *Fuel* **2021**, *293*, No. 120440.
(12) Deng, J.; Ren, P.; Deng, D.; Yu, L.; Yang, F.; Bao, X. Highly Active and Durable Non-Precious-Metal Catalysts Encapsulated in Carbon Nanotubes for Hydrogen Evolution Reaction. *Energy Environ. Sci.* **2014**, *7* (6), 1919−1923.
(13) Ishibashi, K.; Grewal, M. S.; Ito, K.; Shoji, N.; Matsuo, Y.; Yabu, H. Trifunctional Rare-Metal-Free Electrocatalysts Prepared Entirely from Biomass. *Adv. Energy Sustainability Res.* **2022**, *3*, No. 2200107.
(14) Lekitima, J.; Ozoemena, K. I.; Kobayashi, N. Electrochemical Capacitors Based on Nitrogen-Enriched Cobalt (II) Phthalocyanine/Multi-Walled Carbon Nanotube Nanocomposites. *ECS Trans* **2013**, *50* (43), 125−132.
(15) Akyüz, D.; Özçifçi, Z.; Menteşe, E.; Akçay, H. T. Novel Peripheral and Non-Peripheral Oxobenzo[d]Thiazol Substituted Cobalt Phthalocyanines: Synthesis, Electrochemistry, Spectroelectrochemistry, Electrocatalytic Hydrogen Production in Alkaline Medium. *J. Electroanal. Chem.* **2022**, *924* (July), No. 116864.
(16) Morozan, A.; Campidelli, S.; Filoramo, A.; Jousselme, B.; Palacin, S. Catalytic Activity of Cobalt and Iron Phthalocyanines or Porphyrins Supported on Different Carbon Nanotubes towards Oxygen Reduction Reaction. *Carbon N Y* **2011**, *49* (14), 4839−4847.
(17) Morlanés, N.; Joya, K. S.; Takanabe, K.; Rodionov, V. Perfluorinated Cobalt Phthalocyanine Effectively Catalyzes Water Electrooxidation. *Eur. J. Inorg. Chem.* **2015**, *2015* (1), 49−52.
(18) Sakthinathan, I.; Mahendran, M.; Krishnan, K.; Karuthapandi, S. Selenium Tethered Copper Phthalocyanine Hierarchical Aggregates as Electrochemical Hydrogen Evolution Catalysts. *Sustain Energy Fuels* **2021**, *5* (14), 3617−3631.
(19) Abe, H.; Hirai, Y.; Ikeda, S.; Matsuo, Y.; Matsuyama, H.; Nakamura, J.; Matsue, T.; Yabu, H. Fe Azaphthalocyanine Unimolecular Layers (Fe AzULs) on Carbon Nanotubes for Realizing Highly Active Oxygen Reduction Reaction (ORR) Catalytic Electrodes. *NPG Asia Mater.* **2019**, *11* (1), 53.
(20) Zhang, D.; Hirai, Y.; Nakamura, K.; Ito, K.; Matsuo, Y.; Ishibashi, K.; Hashimoto, Y.; Yabu, H.; Li, H. Benchmarking PH-Field Coupled Microkinetic Modeling against Oxygen Reduction in Large-Scale Fe-Azaphthalocyanine Catalysts. *Chem. Sci.* **2024**, *15* (14), 5123−5132.
(21) Yabu, H.; Nakamura, K.; Matsuo, Y.; Umejima, Y.; Matsuyama, H.; Nakamura, J.; Ito, K. Pyrolysis-Free Oxygen Reduction Reaction (ORR) Electrocatalysts Composed of Unimolecular Layer Metal Azaphthalocyanines Adsorbed onto Carbon Materials. *ACS Appl. Energy Mater.* **2021**, *4* (12), 14380−14389.

Downloaded from pubs.acs.org/aaemcq/article-pdf/7/22/10466/18573985/ae4c02102.pdf by DOKUZ EYLUL UNIV user on 01 September 2026

(22) Ishibashi, K.; Ito, K.; Yabu, H. Rare-Metal-Free Zn−Air Batteries with Ultrahigh Voltage and High Power Density Achieved by Iron Azaphthalocyanine Unimolecular Layer (AZUL) Electrocatalysts and Acid/Alkaline Tandem Aqueous Electrolyte Cells. *APL Energy* **2023**, *1* (1), No. 016106.
(23) Ishibashi, K.; Ono, S.; Kamei, J.; Ito, K.; Yabu, H. Rare-Metal-Free High-Performance Water-Activated Paper Battery: A Disposable Energy Source for Wearable Sensing Devices. *RSC Applied Interfaces* **2024**, *1* (3), 435−442.
(24) Hirai, Y.; Ishibashi, K.; Oku, K.; Ito, K.; Yabu, H. Rare-Metal-Free Hydrogen Evolution Reaction Electrocatalysts Based on Metal Azaphthalocyanine Molecular Layer for Anion Exchange Membrane Water Electrolysis. *Discovery Chem. Eng.* **2024**, *4* (1), 13.
(25) Ishibashi, K.; Hirai, Y.; Oku, K.; Ito, K.; Yabu, H. A Molecular Adsorption Concept for Increasing Energy Density of Hybrid Supercapacitors. *ACS Appl. Mater. Interfaces* **2024**, *16* (26), 34393−34401.
(26) Abbaspour, A.; Norouz-Sarvestani, F.; Mirahmadi, E. Electrocatalytic Behavior of Carbon Paste Electrode Modified with Metal Phthalocyanines Nanoparticles toward the Hydrogen Evolution. *Electrochim. Acta* **2012**, *76*, 404−409.
(27) Kumar, Y.; Kibena-Põldsepp, E.; Kozlova, J.; Kikas, A.; Käärik, M.; Aruväli, J.; Kisand, V.; Leis, J.; Tamm, A.; Tammeveski, K. Bimetal Phthalocyanine-Modified Carbon Nanotube-Based Bifunctional Catalysts for Zinc-Air Batteries. *ChemElectroChem.* **2021**, *8* (14), 2662−2670.
(28) Chen, R.; Li, H.; Chu, D.; Wang, G. Unraveling Oxygen Reduction Reaction Mechanisms on Carbon-Supported Fe-Phthalocyanine and Co-Phthalocyanine Catalysts in Alkaline Solutions. *J. Phys. Chem. C* **2009**, *113* (48), 20689−20697.
(29) Alzate-Carvajal, N.; Bolivar-Pineda, L. M.; Meza-Laguna, V.; Basiuk, V. A.; Basiuk, E. V.; Baranova, E. A. Oxygen Evolution Reaction on Single-Walled Carbon Nanotubes Noncovalently Functionalized with Metal Phthalocyanines. *ChemElectroChem.* **2020**, *7* (2), 428−436.
(30) Liao, Z.; Wang, Y.; Wang, Q.; Cheng, Y.; Xiang, Z. Bimetal-Phthalocyanine Based Covalent Organic Polymers for Highly Efficient Oxygen Electrode. *Appl. Catal., B* **2019**, *243*, 204−211.
(31) Pham, H. Q.; Pham-Tran, N. N. Topological Insulating Phase in Single-Layer Pentagonal Covalent Organic Frameworks: A Reticular Design Using Metal Phthalocyanine. *Chem. Mater.* **2021**, *33* (12), 4488−4499.
(32) Kumatani, A.; Matsue, T. Recent Advances in Scanning Electrochemical Microscopic Analysis and Visualization on Lithium-Ion Battery Electrodes. *Curr. Opin. Electrochem.* **2020**, *22*, 228−233.
(33) Takahashi, Y.; Kobayashi, Y.; Wang, Z.; Ito, Y.; Ota, M.; Ida, H.; Kumatani, A.; Miyazawa, K.; Fujita, T.; Shiku, H.; Korchev, Y. E.; Miyata, Y.; Fukuma, T.; Chen, M.; Matsue, T. High-Resolution Electrochemical Mapping of the Hydrogen Evolution Reaction on Transition-Metal Dichalcogenide Nanosheets. *Angew. Chem.* **2020**, *132* (9), 3629−3636.
(34) Kumatani, A.; Ogawa, H.; Endo, T.; Lustikova, J.; Ida, H.; Takahashi, Y.; Miyata, Y.; Ikuhara, Y.; Shiku, H.; Wakayama, Y. Emergence of Electrochemical Catalytic Activity via an Electrochemical-Probe on Defective Transition Metal Dichalcogenide Nanosheets. *APL Energy* **2024**, *2* (1), No. 016107.
(35) Krzywiecki, M.; Grządziel, L.; Juszczyk, J.; Kaźmierczak-Bałata, A.; Erbe, A.; Bodzenta, J. Correlation between Morphology and Local Thermal Properties of Iron (II) Phthalocyanine Thin Layers. *J. Phys. D: Appl. Phys.* **2014**, *47* (33), No. 335304.
(36) Miller, C. W.; Sharoni, A.; Liu, G.; Colesniuc, C. N.; Fruhberger, B.; Schuller, I. K. Quantitative Structural Analysis of Organic Thin Films: An x-Ray Diffraction Study. *Phys. Rev. B Condens Matter Mater. Phys.* **2005**, *72* (10), No. 104113.
(37) Xu, Y.; Li, F.; Xu, A.; Edwards, J. P.; Hung, S. F.; Gabardo, C. M.; O'Brien, C. P.; Liu, S.; Wang, X.; Li, Y.; Wicks, J.; Miao, R. K.; Liu, Y.; Li, J.; Huang, J. E.; Abed, J.; Wang, Y.; Sargent, E. H.; Sinton, D. Low Coordination Number Copper Catalysts for Electrochemical CO2Methanation in a Membrane Electrode Assembly. *Nat. Commun.* **2021**, *12* (1), 2932.
(38) Hong, X. S.; Huo, D.; Jiang, W. J.; Long, W. J.; Leng, J. D.; Tong, L.; Liu, Z. Q. Electrocatalytic and Photocatalytic Hydrogen Evolution by Ni(II) and Cu(II) Schiff Base Complexes. *ChemElectroChem.* **2020**, *7* (24), 4956−4962.
(39) Zhou, B.; Zhang, Y.; Wang, T.; Zhou, W.; Liu, J.; Zou, Y.; Tao, L.; Lu, Y.; Wang, S. Room-Temperature Chemical Looping Hydrogen Production Mediated by Electrochemically Induced Heterogeneous Cu(I)/Cu(II) Redox. *Chem. Catalysis* **2021**, *1* (7), 1493−1504.
(40) Scanlon, M. D.; Peljo, P.; Méndez, M. A.; Smirnova, E.; Girault, H. H. Charging and discharging at the nanoscale: Fermi level equilibration of metallic nanoparticles. *Chem. Sci.* **2015**, *6* (5), 2705−2720.
(41) Güell, A. G.; Cuharuc, A. S.; Kim, Y.-R.; Zhang, G.; Tan, S.-Y.; Ebejer, N.; Unwin, P. R. Redox-Dependent Spatially Resolved Electrochemistry at Graphene and Graphite Step Edges. *ACS Nano* **2015**, *9* (4), 3558−3571.
(42) Kumatani, A.; Miura, C.; Ida, H.; Takahashi, Y.; Ikuhara, Y.; Shiku, H.; Matsue, T.; Okada, T. Comprehensive electrochemical imaging analyses of redox activities correlated to multilayer graphene and graphite structures. *Electrochem. Acta* **2024**, *499*, No. 144688.
(43) Hill, J. W.; Hill, C. M. Directly visualizing carrier transport and recombination at individual defects within 2D semiconductors. *Chem. Sci.* **2021**, *14* (12), 5102−5112.

Downloaded from pubs.acs.org/aaemcq/article-pdf/7/22/10466/1857398/ae4c02102.pdf by DOKUZ EYLUL UNIV user on 01 September 2026



https://doi.org/10.1021/acsaem.4c02102
*ACS Appl. Energy Mater.* 2024, 7, 10466−10473